Interfacial Entanglements between Glassy Polymers Investigated by Nanofractography with High-Resolution Scanning Electron Microscopy

Shin Horiuchi,* Ayumi Nakagawa, and Yonggui Liao

Nanotechnology Research Institute, National Institute of Advanced Industrial Science and Technology (AIST), 1-1-1, Higashi, Tsukuba, Ibaraki 305-8565, Japan

Toshiaki Ougizawa

Department of Organic and Polymeric Materials, Tokyo Institute of Technology, 2-12-1, Ookayama, Meguro-ku, Tokyo 152-8550, Japan

Received July 17, 2008; Revised Manuscript Received September 12, 2008

ABSTRACT: Fracture surfaces created during the interfacial failure of weak interfaces between glassy polymers were investigated with high-resolution scanning electron microscopy (HR-SEM). As reported in an earlier communication (*Macromol. Rapid Commun.* 2007, *28*, 915−921), we found that interfacial failures between immiscible polymers produced large number of nanosized fibrils on the fracture surfaces. In order to investigate the mechanism of such ultra small structure formation in the crack propagation process, welding experiments of monodispersed polystyrenes with different molecular weights were employed by the asymmetric double cantilever beam (ADCB) test. The "nano-fibrils" were produced during the fractures of the interfaces between polystyrenes with the molecular weight higher than 2000, of which thickness was comparable to the entanglement spacing. It was found that the "nano-fibrous" formation bearing in the crack propagation reflected the local entanglement structures formed at narrow interfaces comparable to the entanglement spacing.

Introduction

Correlation between the structure of polymer chains at an interface and its resistance to crack propagation are important both from practical application and scientific investigation point of views. It has been recognized that adhesion between polymers, which is a common parameter for evaluating the interfacial properties, is controlled by intermolecular chain entanglements across the interface.[1−7] The chain coupling across an interface can provide physical links where even immiscible polymers can be made to adhere to each other. A simple calculation of the work of adhesion based on surface and interfacial energies between two polymers is on the order of mJ/m^2, however experimental adhesion values are on the order of a few Joules to several hundred Joules per square meter.[8] For example, the work of adhesion between polystyrene (PS) and poly(methyl methacrylate) (PMMA) was estimated to be 78.6 mJ/m^2,[8] while the measured interfacial toughness was 12 J/m^2.[2] This means that the contribution of entanglements on the toughness of interface is significantly large. The adhesion between welded plastic parts has been evaluated through the measurements of the interfacial fracture toughness (G_c) using asymmetric double cantilever beam (ADCB) geometry.[9,10] This method has proved to be a simple but effective way of testing the strength of the interface between two polymer sheets. By studying the correlation between G_c and interfacial thickness in many polymer systems, where entanglements are the primary sources for adhesion, it has been revealed that there are three regimes associated with failure mechanism: chain scission, chain pull out, and crazing.[2,4] In the welding of a polymer to itself, a sharp transition from chain pull out (or scission) to crazing takes place when the interfacial thickness exceeds a critical value that is closely related to the entanglement distance.[1]

Experimental studies on interface−adhesion relationships have been carried out mainly by neutron reflectivity,[1,2,11] secondary ion mass spectroscopy (SIMS),[12,13] X-ray scattering[14,15] and forward recoil spectrometry (FRES).[16] We previously reported in a communication that high-resolution scanning electron microscopy (HR-SEM) with an in-lens detector system has a potential for providing deeper understanding of interfacial structures and fracture mechanism.[17] Conventional SEM can read topographic surface features only in micrometer scales, allowing us only to do macroscale fractography studies and provide limited information on the deformation and fracture of polymeric materials. We found that the fractured interfaces of immiscible polymer pairs of PMMA and styrene−acrylonitrile random copolymer (SAN) produced a large number of nanosized fibrils.[16] Such ultrasmall features were not observed even though many studies on adhesion-interface correlation have been performed. In the conventional SEM, the secondary electron (SE) detector, located outside of the column, collects all the SEs coming from the different scattering processes, which results in the loss of image resolution.[18] On the other hand, an in-lens detector system, which is equipped in an objective lens as an annular detector, can capture the SEs that are sensitive to the surface topography where the SEs are amplified by a beam booster.[19−21] This allows us to perform high-resolution and high-contrast surface imaging, giving a great large amount of information on surface topography and composition.

Classical fractography limits our capability to study fracture mechanisms at micrometer scales, while HR-SEM extends this capability to investigate fracture behavior and entanglement structures by imaging at nano- and molecular scales, which allows us to perform "nanofractography". PMMA and SAN is a good combination for studying the interfaces between the two polymers because the miscibility between the two polymers can be tuned by varying the random copolymer composition.[22,23] However, the distributions of the composition and molecular weight in the random copolymers limit more detailed studies on correlation between interfacial structures and the "nano-fibrous" pattern. In this work, we employed welding experiments

* Corresponding author. Telephone: +81-29-861-6281. Fax: +81-29-861-4773. E-mail: s.horiuchi@aist.go.jp.

10.1021/ma801607k CCC: $40.75
Published on Web 10/14/2008

using simple monodispersed polystyrenes by varying the welding time and the molecular weight. Here, the interfacial structures in terms of the thickness and the entanglement were discussed, comparing with the results of the PMMA/SAN system.

Experimental Section

Materials. Monodispersed PS with different molecular weights were purchased from Polymer Source Inc. (Canada) and used as received. PMMA was purchased from Wako Chemical Co. Ltd., (Japan). The weight average molecular weight (M_w) and the molecular weight distribution (M_w/M_n) of PMMA were 113 kg/mol and 2.1, respectively. SAN copolymers containing acrylonitrile (AN) of 29 wt % and 34 wt % (SAN29 and SAN34, respectively) were used without any further purification, of which M_w were 213 and 130 kg/mol, and M_w/M_n were 2.4 and 2.3, respectively. Bisphenol A polycarbonate (PC) was supplied from Teijin Chemicals Ltd. (Japan) under a product name of Panlite1250Y of which M_n was 25 kg/mol.

Measurements of Interfacial Toughness. The interfacial adhesion strength was evaluated by ADCB test. The detailed procedure and the effectiveness of this method for the evaluation of interface toughness are described elsewhere.[9,10] PS, PMMA and SAN were compression molded between silicon wafers into sheets to obtain smooth surfaces at 170 °C, while PC was molded at 200 °C. Monodispered PS's with M_w's below 5000 were difficult to be molded into the sheet due to their brittleness. In such cases, a 50 wt % PS concentrated toluene solution was coated to a thickness of 30 μm on a SAN sheet (SAN is not dissolved in toluene) by using a bar-coater. Two slabs (1 cm × 5 cm) were laminated above the glass transition temperatures (T_g) for different periods in nitrogen atmosphere. To ensure the good contact between the two surfaces, two slabs were joined together under slight pressure for the first 15 min. After quenching the specimen to room temperature to freeze the interdiffusion, a razor blade was driven into the interface between the two polymer sheets to propagate an interfacial crack. When the crack propagation stopped, the length ahead of the blade was measured under a microscope. The interfacial toughness, G_c, was then calculated. The mean values were calculated with at least ten data points for each laminate. The beam width of PS/PS symmetric laminates was 1.5 mm. For the asymmetric cases (PMMA/SAN and PC/SAN), G_c values were calculated by varying the thickness of the PMMA or PC beams from 1.7 to 2.3 mm with a fixed thickness of SAN at 1.7 mm. Based on these measurements, a minimum G_c value was found, which was considered to be the true interfacial toughness.

SEM. A Carl Zeiss ULTRA55 field emission scanning electron microscope (Carl Zeiss SMT, Oberkochen, Germany), integrating the in-lens detector system, was operated at an accelerating voltage of 2 kV for the observation of fracture surfaces produced by ADCB tests. The details of the principle of this system appear elsewhere. To avoid the charging problem, the samples were coated with osmium using an OP80NT osmium plasma coater (Filgen Inc., Japan) with OsO_4 as the source material.

In order to image the structure underneath the fracture surfaces by SEM, "Surface and Interface Cutting Analysis System" (SAICAS) NN-40 (Daipla Wintes Co., Ltd., Japan), which is an extremely low angle gradient shaving instrument, was used. The fracture surfaces were shaved with SAICAS using a diamond blade, operated by piezoelectric actuator, with the vertical and horizontal velocities of 50 and 1000 nm/s, respectively. Then, the internal structure underneath the surface was exposed as a slope surface with a low gradient that could be easily accessed by SEM.

Energy-Filtering Transmission Electron Microscopy (EFTEM). Transmission electron microscopy (TEM) study and elemental mapping were carried out using an energy-filtering transmission electron microscope, LEO922 (Carl Zeiss SMT, Oberkochen, Germany), which is equipped with an LaB_6 cathode and an Omega-type energy filter. The microscope was operated at an accelerating voltage of 200 keV.

The interfaces of PMMA/SAN were investigated by elemental mapping as reported in our previous papers.[17,24] The preparation of the specimens for TEM by ultramicrotomy was performed by carefully adjusting the angle between the diamond knife and the interface to 90° with knife stroke parallel to the interface. For the focus adjustment during the TEM operation and the drift correction for the element mapping, gold nanoparticles with 10 nm diameter were dispersed onto the thin sections using dilute gold colloid aqueous solution. All observations were performed cryogenically at 120 K. For cross sectional views of the fracture surfaces, the fractured ADCB specimens were again laminated using a visible-light curable resin, Clear Luce MA21 (Adell Corp., Japan), and were cut by ultramicrotomy.

X-ray Photoelectron Spectroscopy (XPS). The XPS analyses were performed by a Perkin-Elmer PHI5600 ESCA system with an Al Kα X-ray source, and the emitted electrons were detected at 16 kV, 30 W power, 150 μm spot size, and a 45° takeoff angle.

Results and Discussion

Analysis of Fracture Surfaces by SAICAS−SEM and XPS. It has been well-known that a random copolymer has a favorable interaction in its blends with a homopolymer, giving high miscibility even when each component of a random copolymer has poor miscibility with a homopolymer. The interaction parameters, χ, of a homopolymer/random copolymer blend systems can be tuned by varying the random copolymer composition, and are sometimes negative when the random copolymer composition is in a certain range, giving miscible blends. Both PMMA/SAN and PC/SAN blends exhibit minimums in the χ parameter when the AN content in SAN is varied.[25] PMMA/SAN blends show negative χ parameter around the minimum and thus become miscible when the AN content is between 10 and 33 wt %,[26] while the χ parameters of PC/SAN blends are positive even at the minimum and are immiscible at all the AN contents in SAN.[27]

The fracture behaviors of PMMA/SAN and PC/SAN are quite different from each other as shown in Figure 1, where the fracture surfaces of SAN29 after ADCB test at 140 °C for 2 h are shown at three different magnifications. The G_c values of PMMA/SAN29 and PC/SAN29 were 290 and 10 J/m^2, respectively. The difference in the miscibility of those two systems results in a significantly large difference in terms of the interfacial toughness. The PMMA/SAN29 forms thick interface *via* interdiffusion and thus gives a high G_c value. As shown in Figure 1a−c, the fracture surface exhibits a macroscopically rough pattern with appearance similar to those of bulk amorphous polymers. The surface is covered with a large number of dimples with the diameter of approximately 5 μm. There seems to be a nucleation site at the center of each dimple as shown in Figure 1c. Micro voids may be produced ahead of the main crack, and then these coalesce to enhance the progress of the crack. Such a dimple pattern on a fracture surface is interpreted to be formed as the combination of the primary crack front, which is originated by the separation process of the interface, and the secondary crack, which is produced by the nucleation of the micro voids ahead of the primary crack.[28] The PC/SAN29, on the other hand, has a weak interfacial toughness due to its immiscibility. The fracture surface was thus quite smooth and showed no topographic features at micrometer scale (Figure 1d). However, HR−SEM allowed us to see the formation of nanofibrils of approximately 20 nm in size as shown in Figure 1, parts b and c. As was reported in our previous communication, this kind of fibrous structure was also produced during the fracture of PMMA/SAN34 and PMMA/SAN40 immiscible systems. XPS spectra of the fracture surfaces of PMMA/SAN29 and PC/SAN29 are shown in parts a and b of Figure 2,

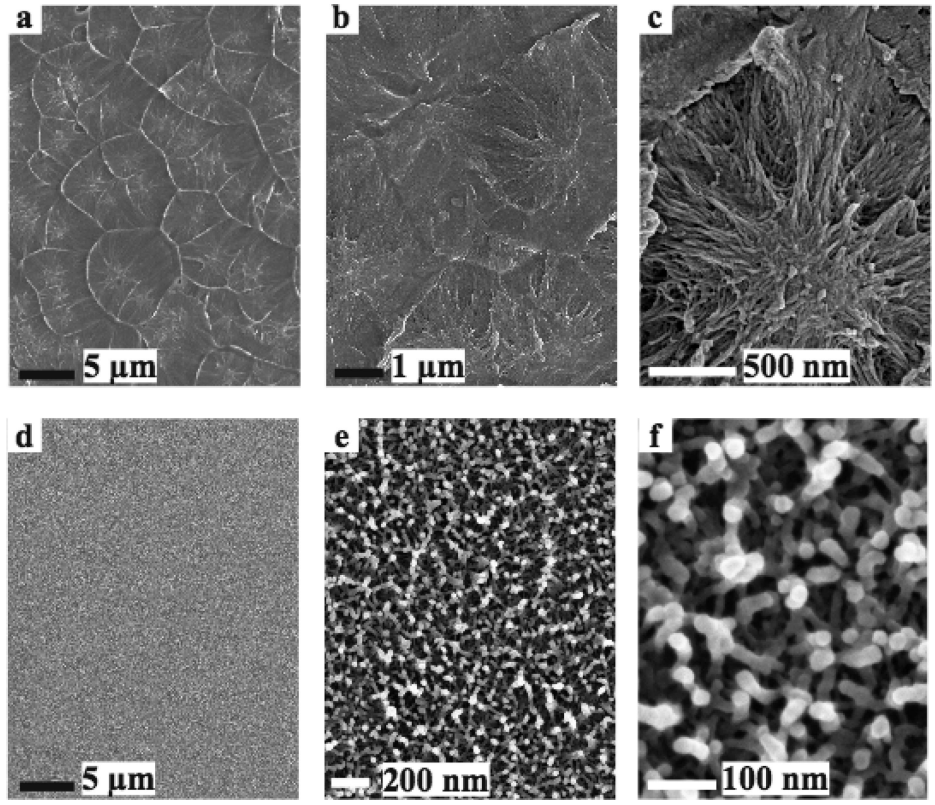

Figure 1. SEM micrographs showing the fracture surfaces of PMMA/SAN29 (a-c) and PC/SAN29 (d-f) laminates. All the micrographs were taken from the surface of the SAN29 sheets. The magnification increases from the left to the right.

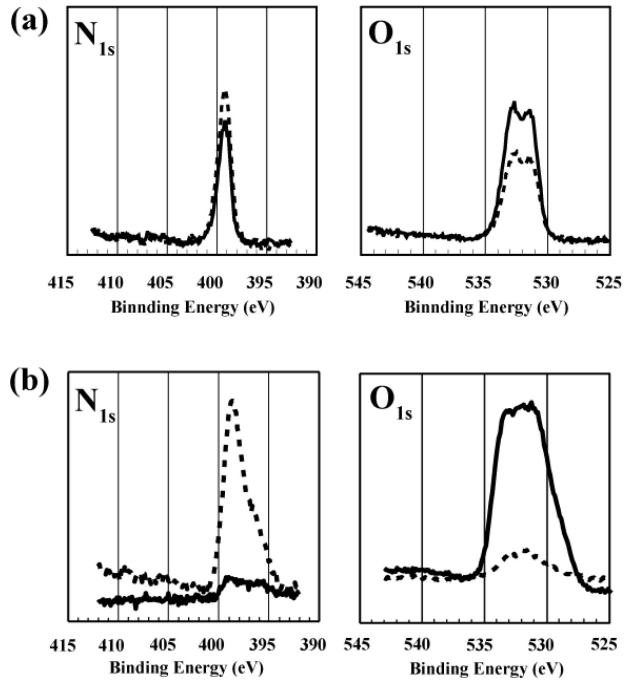

Figure 2. N_{1s} and O_{1s} XPS spectra acquired from the fracture surfaces of (a) PMMA/SAN29 and (b) PC/SAN29 laminates. Solid lines correspond to the spectra from SAN29 surface side, while the dotted lines correspond to the PMMA side (a) and the PC side (b).

respectively. Both the XPS N_{1s} and O_{1s} peaks appear on the both sides with the comparable intensities on the fracture surfaces of the PMMA/SAN29 laminate, while the SAN29 side is extremely rich in nitrogen and the PC side is *vise versa* in the PC/SAN29 laminate. This indicates that the fracture mode of the two systems is considerably different from each other: (1) cohesive fracture of the PMMA/SAN29 interface, where the failure occurs within the thick interfacial layer, and (2) interfacial fracture of the PC/SAN29 interface, where the failure occurs at the interface. Therefore, we could observe the similar transition from the micrometer-scale "dimple pattern" to the "nano-fibrous pattern" with the change in the miscibility, as shown in the previous study using the PMMA/SAN system with various AN contents in SAN.[17]

The molecular events that occur in the fracture process of those two systems are interpreted as follows: The polymer chains at the PMMA/SAN29 interface are sufficiently entangled, and thus the interface is strong enough to produce a plastic deformation at the crack front, dissipating a huge amount of energy before the interface fails. Crazing occurs in the plastic deformation region, which leads to the formation of interpenetrating microvoids and cross-ties fibrils. The XPS results suggest that the drawn fibrils are finally broken by chain scission. The polymer chains at the PC/SAN29 interface, on the other hand, are not mutually entangled, and thus fail exclusively by chain pullout. The fracture toughness of the PC/SAN29 interface (10 J/m^2) seems to be much small, but it is significantly larger than a work of adhesion calculated by surface and interfacial energies, which is on the order of mJ/m^2. Therefore, it is assumed that the fracture energy is dissipated for the nanoscopic deformation in the chain pull out process.

This ultrasmall fibrous feature has hardly been seen by conventional SEM or by atomic force microscopy. One may suspect that this ultrasmall fibrous structure is produced by electron beam irradiation during the SEM observation or during the osmium plasma coating process. In fact, the structure is truly produced during the fracture process which has been confirmed by employing SAICAS-SEM technique.[29−31] As illustrated in Figure 3a, a surface of the specimen was shaved with a diamond blade with an extremely low angle. The cutting angle to the surface in this condition was 2.9°. Figure 3b shows the shaved

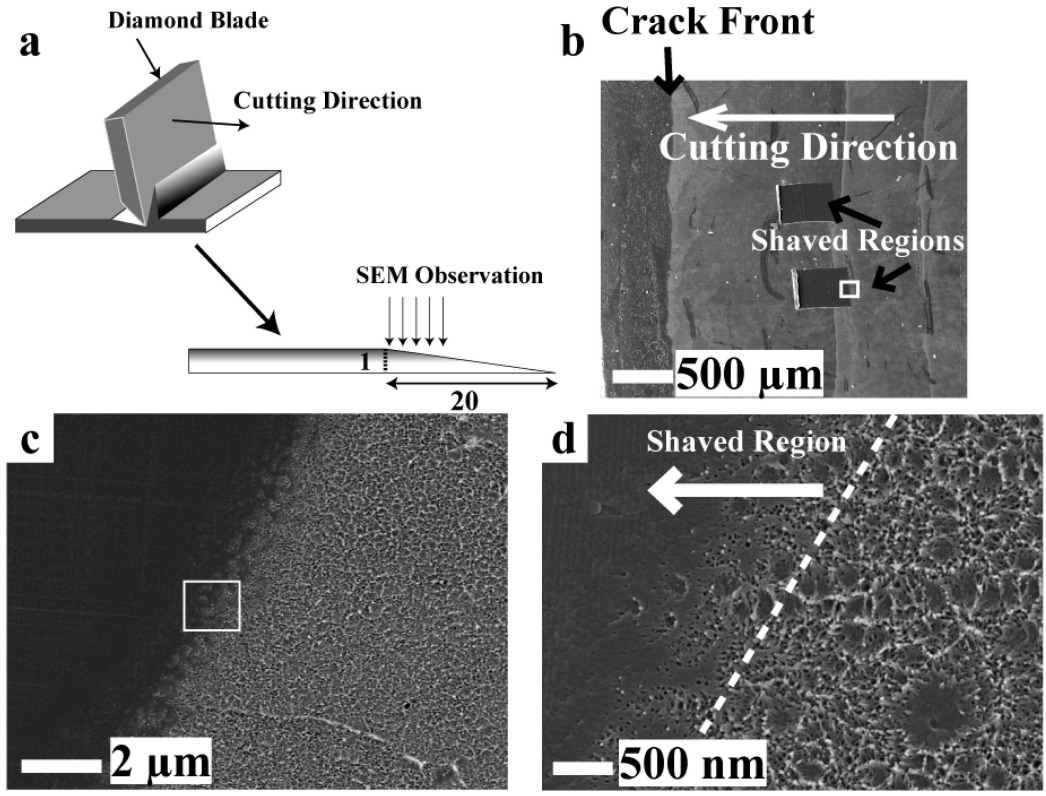

Figure 3. (a) Schematic illustration of gradient shaving preparation method. (b−d) SEM micrographs showing the shaved region of SAN29 fracture surface of the PC/SAN29 lamination.

regions created on the fracture surface of SAN29 shown in Figure 1d−f. Parts c and d of Figure 3 are zoomed images of the region where the cutting started. The shaved region presents the amplified structure underneath the fracture surface, showing that the fibrils' layer is formed only in the narrow region underneath the original surface with a width of approximately 700 nm on the gradient slope. Therefore, the real thickness of the produced fibrils' layer is estimated roughly to be 35 nm (=700 nm × sin 2.9°). The shaved region exhibited smooth surface with no fibrils, indicating that the "nano-fibrous" pattern is not an artifact caused by the electron beam irradiation or by the plasma exposure.

"Nano-Fibrous" Formation on Monodispersed PS Fracture Surfaces. As stated in the above section, the "nano-fibrous" structure is created during the fracture of the interfaces where the interfacial fracture is a dominant fracture process. In order to find the criteria of the "nano-fibrous" structure formation and its correlation with interfacial entanglement structure, we introduced a simple system, where the two sheets of the same polymer with a narrow molecular weight distribution were welded over different periods at a temperature above T_g. Using such a symmetric system, we can work with a same polymer pair but with varying interfacial thicknesses.

We performed welding experiments between PS/PS with an identical molecular weight in order to study the correlation of the fracture surface patterns with interfacial width and toughness. In this experiment, the polymer chains mutually diffuse across the interface, and the interfacial thickness increases with increase in the welding time. Figure 4 shows a double logarithmic plot of interfacial toughness between PS sheets, of which M_w is 541K and M_w/M_n is 1.07, versus the welding time at 120 °C. HR-SEM images of the fracture surfaces at several welding times are also shown therein. Schnell et al. has investigated the correlation between interfacial adhesion and thickness of PS/PS with the combination of neutron reflectivity and fracture toughness measurement using the ADBS geometry.[1] The interfacial thicknesses between protonated PS (752K) and deuterated PS (660K) measured by neutron reflectivity by their group are also given on the same plot.[32] A problem for the comparison of our results with the reported ones is that the molecular weights used for the thickness measurement in the literature were different from the one used in our experiment. The interfacial thicknesses could be estimated using the scaling law expressed as $d \propto M^{-1}t^{1/2}$, where d, M, and t are interfacial thickness, diffusion time and molecular weight.[33] The molecular weights of the nondeuterated and deuterated PSs used in the literature are averaged to be 706K, and then the interfacial thicknesses in our case are predicted to be about 30% larger than the reported values. However, the time dependence of the interdiffusion in the literature did not exhibit the relationship of $d \propto t^{1/2}$, where a rapid intermixing of chain segments in an initial stage of the diffusion occurred. Therefore, we think that the interfacial thickness in our case should be slightly larger than the reported values but the scaling law may overestimate the thickness. Thus, we used the as-reported interfacial thickness values in the following discussion.

As reported by Schnell et al., there are three stages associated with the G_c dependence on the welding time.[2] In the first stage, G_c is quite low and its increase is less steep with time. In the second stage, G_c drastically increases within a short period and abruptly jumps up to a value close to the toughness of the bulk PS. In the third stage, G_c stays nearly constant and becomes independent of the welding time. Our results also show the same trend, but the fracture toughness values in the initial stage are much lower than the values shown in the literature in which the adhesion energy of 93 J/m^2 was measured already after 6 min. The reported interfacial toughness was measured at different temperatures and reduced to 120 °C using the WLF equation, while all the toughness values in our experiment were measured at 120 °C. The initial stage of polymer interdiffusion

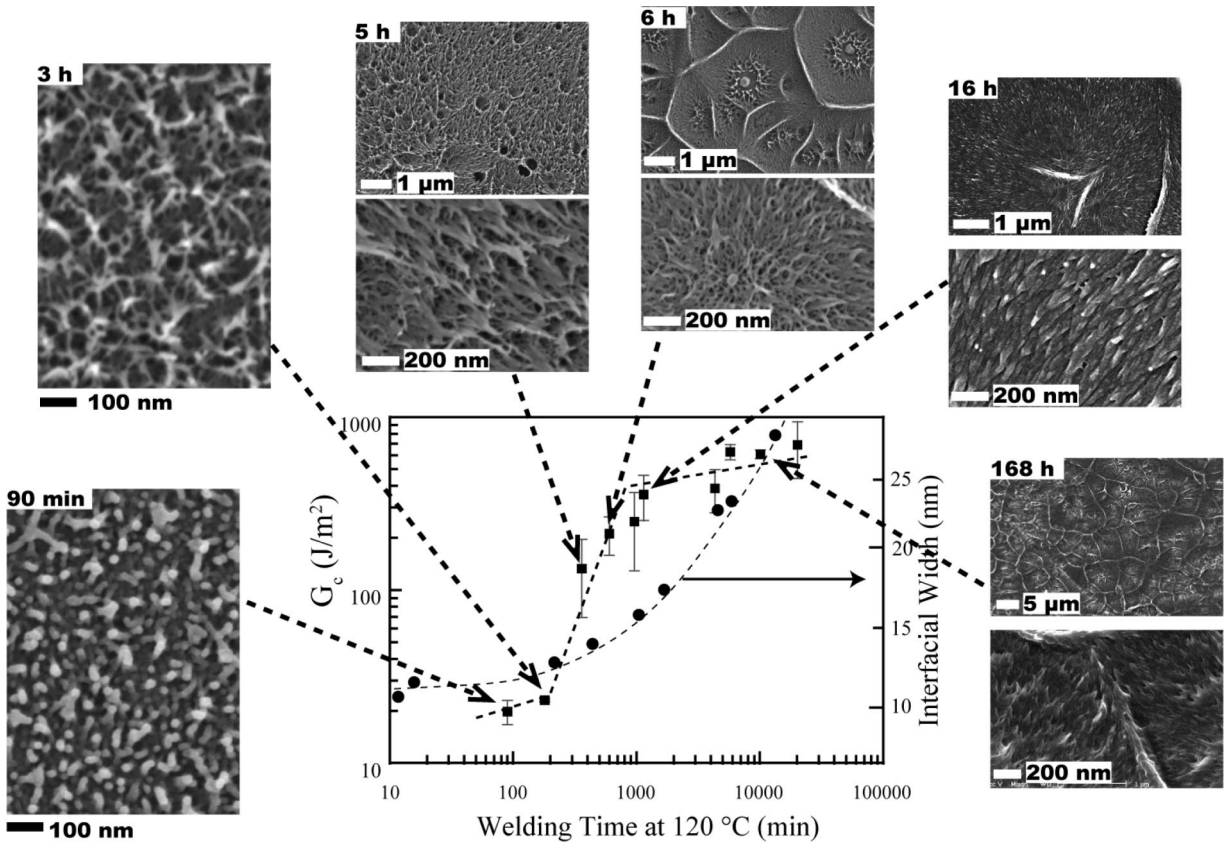

Figure 4. Double logarithmic plot of the interfacial toughness (G_c) of PS/PS 541K vs the welding time at 120 °C, and SEM micrographs showing the fracture surfaces at several welding times. The interfacial thicknesses measured by neutron reflectivity by Stamm et al.[30] are also plotted.

of thick specimens used for the ADCB test may include the period for softening and wetting of the specimens predominantly before the chain interdiffusion was allowed. This induction period is predominantly included in the initial stage, resulting in the relatively low interfacial values. The measured G_c's are, however, comparable to the reported values for various immiscible polymer pairs, where the interfacial thicknesses are less than 10 nm.[2,4] For example, G_c between PS and PMMA is about 12 J/m^2 with the interfacial thickness of 5 nm.[2] Using the reported interfacial thickness values measured by neutron reflectivity, it is learned that the increase in the toughness occurs over a relatively narrow range of interfacial thickness between 9 and 12 nm, and the further interdiffusion of the polymers give no contribution to the toughness enhancement, which represents the same trend as reported by Schnell et al.[1] The HR-SEM images show the dynamic changes in the fracture surface patterns with the welding time, representing how the interfacial toughness relates to the fracture surface. It obviously shows that the "nano-fibrous" pattern is produced in the first stage when the toughness and the interdiffusion are quite low (90 min and 3 h). In the second stage, the fibrils become elongated with increase of G_c (5 h), and then the micrometer scale dimple pattern appears in the later part of the second stage (6 h), with the "nano-fibrils" produced inside the dimples. Finally in the third stage, the "nano-fibrils" disappear and micrometer scale dimple pattern is the dominant feature as was observed in the PMMA/SAN29 miscible system (Figure 1a).

The critical interfacial thickness ranging from 9 to 12 nm, at which a significant increase in the interfacial toughness occurs, is closely related to the average distance between the entanglement points in PS, which was estimated to be 9.3 nm.[34] It means that sufficient interfacial toughness comparable to the bulk polymers can be achieved with narrow interfaces being considerably smaller than the radius of the gyration of the polymers, which is estimated to be 21.3 nm for 570K PS.[1] It also means that the polymer chains need only to penetrate roughly by an entanglement distance for an optimum adhesion. The welding experiment of the monodispersed PS clearly indicates that the "nano-fibrous" fracture surface is created during the fracture of the narrow interfaces formed during the initial stage of the interdiffusion before the drastic increase in the toughness occurs. Therefore, it can be mentioned that the "nano-fibrous" fracture pattern can be formed when the polymer chains are disentangled at the interface where the mechanically effective entanglements cannot be formed.

It has been known that the drastic increase in the interfacial toughness occurs as a result of a shift in the molecular failure mechanism.[2] As the interfacial thickness increases, failure mechanism changes from chain pullout to crazing. Therefore, the "nano-fibrous" pattern is created when the chain pullout is the dominant fracture mechanism. In the second stage where the interfacial toughness increases drastically with increase of the interfacial thickness, the transition from chain pullout to crazing occurs, and the fracture surface exhibits the mixed features of the "nano-fibrils" and the "dimples".

Silvestri et al. introduced a new fracture regime concept called "partial crazing", corresponding to a situation where the craze can start but not fully developed.[3] In this regime, some of the load-bearing strands are broken during plastic deformation, but cross-tie fibrils are not yet created, so that lateral stress cannot be transferred. Even in the initial stage of the adhesion development, the fracture energies are extremely larger than the work of adhesion as stated in the earlier part, suggesting that there must be plastic deformation for dissipating the large amount of fracture energies. It is anticipated that the nanosized fibrils are representing the plastic deformation created in the partial crazing regime before the complete crazing occurs.

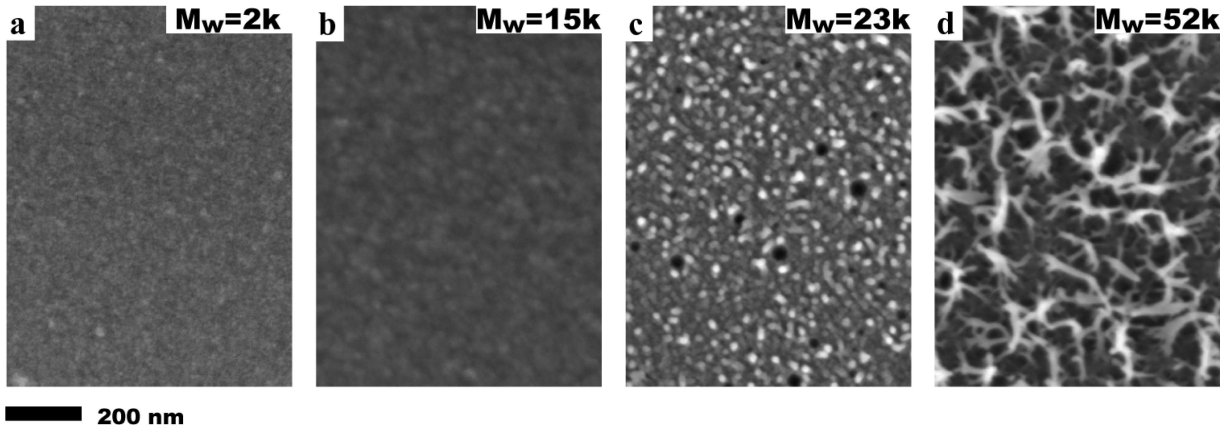

Figure 5. Molecular weight dependence on the fracture surfaces of PS welded at 120 °C for 3 days. M_w and M_w/M_n are (a) 2K and 1.06, (b) 15K and 1.06, (c) 23K and 1.03, and (d) 52K and 1.04.

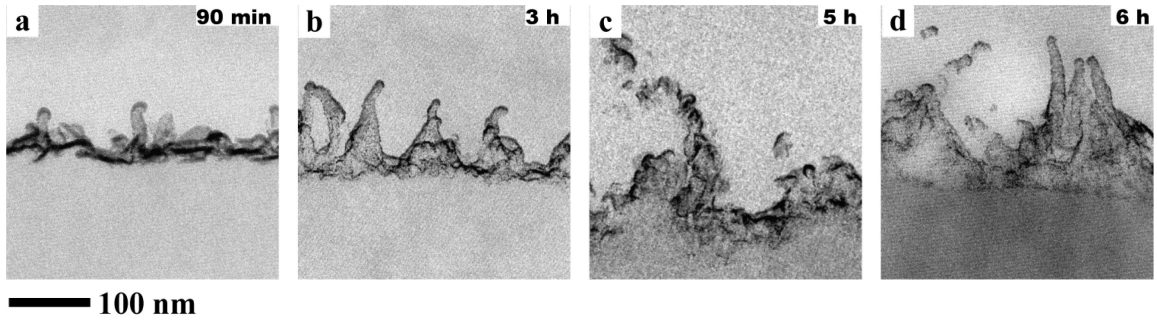

Figure 6. Cross sectional TEM images showing "nano-fibrous" structures of PS fracture surfaces welded for (a) 90min, (b) 3 h, (c) 5 h and (d) 6 h.

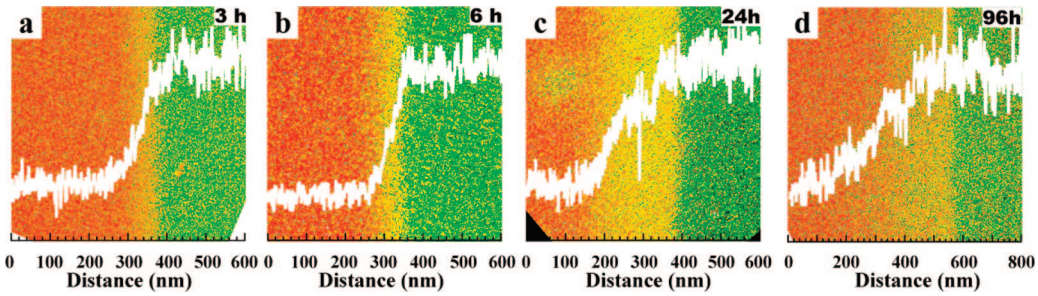

Figure 7. RGB composite images of the oxygen (green) and the nitrogen (red) maps created by EFTEM showing the development of the interface between PMMA and SAN annealed at 140 °C. The SAN is a mixture of SAN29 and SAN34 containing 5 wt % of SAN29. Welding times are (a) 3 h, (b) 6 h, (c) 24 h and (d) 96 h. All images except for (d) are shown at the same magnifications. The ratios of the oxygen to nitrogen concentration profiles across the interfaces, which were calculated from the region with 50 nm widths, are overlapped onto the corresponding images.

Similar drastic increase in toughness accompanied by the transition of failure mechanism from chain pullout to crazing can also be achieved when the molecular weight of the polymer increases.[35] As molecular weights equal to $5-8M_e$, where M_e is the average molecular weight between entanglement points (18 000 for PS),[36] the transition from pullout to crazing occurs. Figure 5 shows the effect of the molecular weight on the fracture surface pattern of PS welded for 3 days at 120 °C. Even though the specimens were welded for such a long time to allow sufficient interdiffusion, no measurable interfacial toughness was obtained. The specimens were entirely separated with a slight insertion of a razor blade into the interface. This means that no mechanically effective entanglements can be formed at the interfaces due to their molecular weights being lower than the critical molecular weight ($5-8M_e$), which is equal to the molecular weight of 90−144K. As shown in Figures 5a and 5b, when the molecular weights are lower than M_e, no specific features are present on the fracture surfaces. When the molecular weight increases to above M_e, the "nano-fibrous" pattern begins to appear as shown in Figure 5c and the fibrils become long with increase of M_n (Figure 5d). These results strongly support our hypothesis that the "nano-fibrils" are the products obtained when the polymer chains are disentangled at the interfaces, and are closely related to the entanglement structures.

Therefore, we conclude that the "nano-fibrous" pattern represents the local entanglement structures at interfaces with narrow widths comparable to the entanglement spacing. Figure 6 shows the changes in the "nano-fibrils" with increase of the welding time as represented by the cross sectional TEM views of the PS ($M_w = 541$K). The fibrils become longer with increase of welding time in the initial stage (Figure 6, parts a and b) and then those seem to form bundles after 6 h (Figure 6) when the dimple pattern appears with increase in the toughness. For the measurements of the interfacial thickness between the identical polymers, it has been required to use a deuterated polymer for one side. The "nano-fibrous" pattern offers the

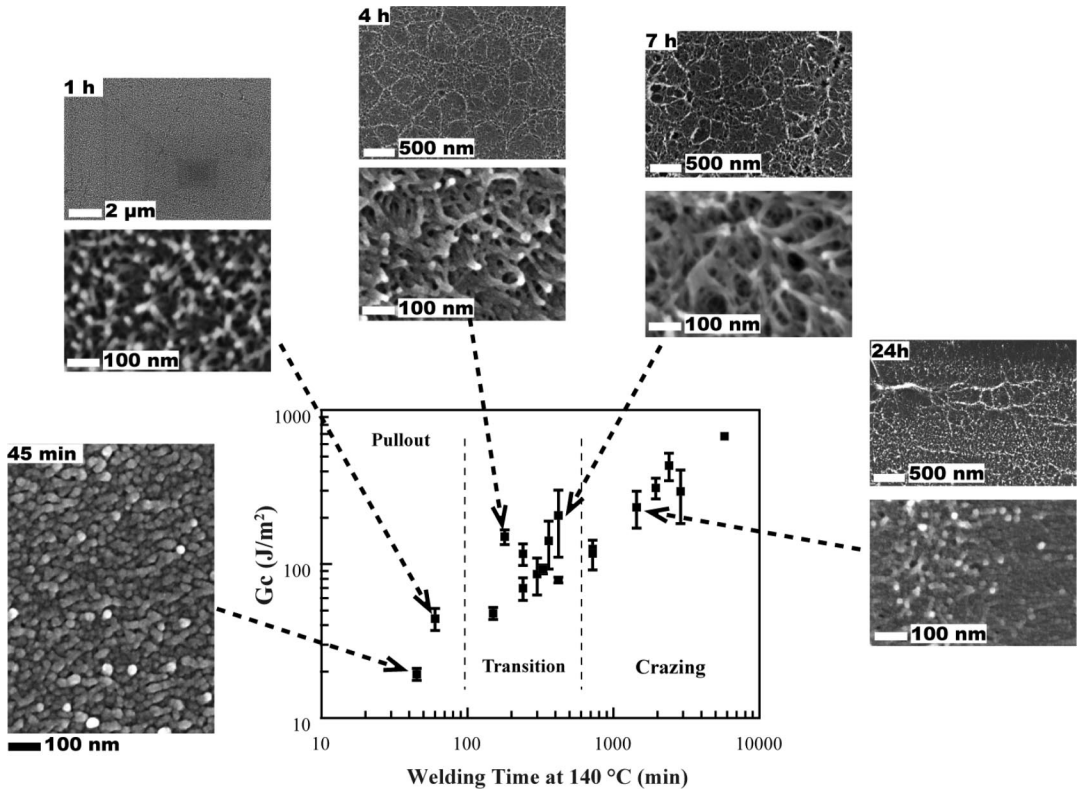

Figure 8. Double logarithmic plot of the interfacial toughness (G_c) of PMMA/SAN versus welding time at 140 °C, and SEM micrographs showing the fracture surfaces at several welding times.

possibility to investigate the local entanglement structures qualitatively including the thickness and mechanical effectiveness without the use of expensive deuterated polymers.

Adhesion Development of PMMA/SAN *via* Segregation of a Miscible Component toward the Interface. The "nanofibrous" pattern on the fracture surface has been well correlated with the PS-PS adhesion development in the initial stage as stated in the above section. However, in many practical adhesion applications, system may be far from an ideal case of the adhesion between monodispersed PS's. Namely, systems usually include multicomponents, broad molecular weight distributions, and different T_gs. In those cases, components having favorable interactions tend to be segregated into interfaces.[13,37] Moreover, the adhesion of the PS−PS is driven only by entropic force, while in most dissimilar polymer pairs, enthalpic force additionally drives the interdiffusion and adhesion. Therefore, miscible polymer pairs have shown rapid interdiffusion and complicated adhesion behaviors in contrast to the interdiffusion of identical polymer pairs.[17,24,26]

Hence, we next investigated the adhesion development which may be caused by the segregation of a component toward the interface by the nanofractography study in PMMA/SAN system, where two SAN's with different AN contents were blended and was put into contact with PMMA. As reported in our previous paper,[17] interfacial toughness of PMMA/SAN29 was more than ten times higher than that of PMMA/SAN34. This drastic enhancement was achieved through the transition of the fracture mode from interfacial to cohesive failure. It is thus predicted that when a SAN29 and SAN34 mixture with SAN34 being the major component is put into contact with PMMA, the small amount of SAN29 would migrates to the interface, providing a variety of interfacial thickness and adhesion strength in a same dissimilar polymer pair.

The two SANs mixture with SAN29 content as 5 wt % was prepared by the precipitation of a toluene solution into large amount of methanol. Then, the PMMA/SAN (29/34) laminates were prepared at 140 °C for different welding times. The interfaces formed via interdiffusion of PMMA and SAN were imaged and the composition profiles of the interfaces were created by EFTEM as reported in our previous works.[17,24] Figure 7 shows RGB composite images of the oxygen (green) and the nitrogen (red) elemental maps that exhibit the interfacial regions as yellow layers due to the composition of the red and green pixels. The composition profiles were also created by calculating the ratio of the intensity profiles across the interface of the two elemental maps. The series of the images shown in Figure 7 represent the growth of the interfacial layer with welding time. The interface between PMMA and the unmixed SAN34 does not form such thick interface,[38] suggesting that the small amount of SAN29, which is miscible with PMMA, migrates to the interface and enriches the interfacial layer. The composition profiles across the interfaces welded for the relatively short periods (Figure 7, parts a and b) show smooth single gradients. On the other hand, with increasing welding time, the profiles at the interfaces became gradual (Figure 7, parts c and d), and seemed to have a plateau in the middle part of the profiles, which is similar to the case of the PMMA/SAN29 interdiffusion.[24] In contrast to the PS−PS welding results, this system exhibits rapid interdiffusion and forms extremely thick interfaces within the short periods.

Figure 8 shows the result of the welding experiments of PMMA/SAN(29/34), showing a double logarithmic plot of G_c versus welding time at 140 °C. HR−SEM images of the fracture surfaces of the SAN side at several welding times are also presented therein. The behavior of the adhesion development with welding time in PMMA/SAN(29/34) system significantly differs from that in the PS-PS adhesion. That is, the toughness of the interface increases continuously with the welding time, and does not show the S-shaped curve as shown in the PS−PS adhesion development (Figure 4) where the toughness jumped

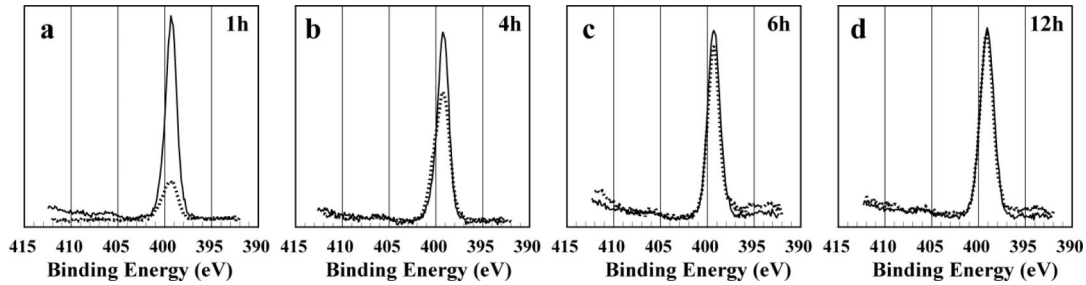

Figure 9. N_{1s} XPS spectra acquired from the fracture surfaces of PMMA/SAN laminates welded for (a) 1 h, (b) 4 h, (c) 6 h, and (d) 12 h. The solid and dotted lines correspond to the SAN and the PMMA sides of the laminates.

up to the bulk toughness with increase of the interfacial thickness. Moreover, the interfacial thicknesses of PMMA/SAN(29/34) system are significantly wider than those of the PS−PS. The diffusion of the two dissimilar polymers was more rapid than those between identical polymers owing to the enthalpic driving force. The interface toughness, however, could not reach to the bulk values in the early stage but it did continue to increase even though the wide interfacial zone for the full entanglement of the polymer chains had been established. Finally, the interfacial toughness did reach to the level of the bulk toughness (500 J/m^2), but even after that it still seemed to continue to increase. Then, no cracks were produced ahead of the razor blade along the interface, and the crack was kinked out of the interface, resulting in the breakage of relatively weak PMMA sheet. The same tendency has been observed in the adhesion of a miscible polymer pair of PMMA/SAN29, and the discrepancy of this adhesion development from that of the PS/PS interface has been discussed in our previous paper.[24] It was speculated that the interdiffusing polymer chains are not able to form entanglements which are mechanically as effective as in the bulk phase in the early stage of the diffusion even with their thick interfaces.

In this study, we discuss this unique adhesion behavior by means of fractography. HR−SEM images shown in Figure 8 indicate that similar changes in the appearance of the "nano-fibrous" patterns with welding time can be observed as in the PS−PS adhesion development. The "nano-fibrils" appear uniformly on the fracture surface in the early stage of the welding, and the fibrils become longer with time. Then, micrometer-scale dimples appear in the middle stage with the elongated fibrils inside of the dimples. Finally, the fibrils disappear and macroscale rough surface is presented. Considering these features, the adhesion development process can be divided in the three stages in terms of the failure mechanism as indicated in the figure. XPS analysis of the fracture surfaces quantitatively represents the changes in the failure mechanism in the adhesion development process. Figure 9 shows the XPS N_{1s} peaks acquired from the SAN and the PMMA sides at several welding times, where the solid and the dotted lines correspond to the SAN and the PMMA sides, respectively. The N_{1s} peak intensities of the two sides show significant difference in the initial stage (Figure 9a), indicating that the interfacial fracture occurs with the chain pullout being the dominant mechanism as a molecular event. With increase of welding time, the N_{1s} peak intensity on the PMMA side gradually increases (Figure 9, parts b and c) and finally become the same as that on the SAN side (Figure 9d), which means that the crack propagates within the thick interfacial layer. At the later stage of the adhesion development, the polymer chains with high molecular weight are sufficiently entangled to initiate the crazing. The crazing process begins with the formation of microvoids and fibrils, which fail through a scission event, giving the comparable intensities of N_{1s} peaks.

As shown in Figure 7, the interfacial thicknesses are considerably larger than the gyration of the polymer chains even in the beginning of the adhesion and the full entanglement of the high molecular weight polymer chains could be included there. However, the interfacial toughness is much lower than the toughness of the bulk and is continuously increasing with increase of the welding time. The formation of the "nano-fibrils" indicates that the chain pullout occurs even when the interface is wider than 100 nm. This suggests that mechanically effective entanglements cannot be formed within the interfacial layer. The materials used in this experiments have broad molecular weight distributions and moreover, the random copolymer SAN may have compositional distributions. The thick interfaces are formed presumably due to the segregation of low molecular weight species of the both polymers and SAN components with a favorable interaction with PMMA. Therefore, the polymer chains in the interface cannot sufficiently be entangled to each other. In this case, the interfacial thickness does not determine the toughness of the interface.

Conclusions

HR-SEM allows us to perform fractography study with high-resolution features that are smaller by 2 orders of magnitude than can be attained by conventional SEM. The welding experiment of monodispersed PS sheets revealed that ultrasmall fibrils with diameter of about 20 nm are produced on the surface fractured via simple chain pullout mechanism. As for the interface between monodispersed PS sheets, it has been known that interfacial toughness was well correlated with the interfacial thickness. "Nano-fibrous" fracture pattern appears before the occurrence of large increase in the toughness. This means that the pattern can be formed when the polymer chains are disentangled at an interface where the mechanically effective entanglements for crazing cannot be formed. With the development of adhesion, the mixed features of "nano-fibrous" and "dimple" pattern seemed to appear. This indicates that the change in the fracture surface from "nano-fibrous" to "dimple" can be attributed to the change in the molecular failure mode from chain pullout to crazing. In other words, nanofibrils are formed in the situation where polymer chains are not effectively entangled for the development of the complete crazing, which is called as "partial crazing". The fracture energies in the initial stage of the adhesion are much lower than that by crazing, but those are more than ten times larger than the energies calculated by a work of adhesion. This large excess energy may be dissipated by the formation of the nanofibrils.

On the other hand, the adhesion development of the PMMA/SAN interface via segregation of the miscible component in SAN did not show any sharp transition in the dependence of G_c on the welding time. In this case, considerably wide interfaces could be obtained but G_c could not reach to the level of the toughness in the bulk polymers. The interfacial thickness does not determine the toughness. However, the growth of the "nano-fibrils" with welding time allows us to understand how the mechanical effectiveness of the entanglements is developed at

the interface. It is, therefore, speculated that low molecular weight polymers and the SAN with a favorable interaction with PMMA are migrated preferentially toward the interface, which reduces the entanglement density and facilitates chain pullout.

We here show that the electron microscopy techniques have the capability to investigate the entanglement structures formed at interfaces. It is indicated that the "nano-fibrous" patterns formed via interfacial fracture represent the local entanglement structures. We expect that the nanofractography study with HR-SEM presented here has a potential to investigate the qualitative local entanglement structures in terms of mechanical resistively against fracture and topological features. Moreover, quantitative analysis in terms of the fibril length and width will lead to the quantitative characterization of the entanglement structures at weak interfaces.

Acknowledgment. We thank Prof. Atsushi Takahara and Kazuyuki Oya, Institute for Materials Chemistry and Engineering, Kyushu University, for the support of the SAICAS measurements.

References and Notes

(1) Schnell, R.; Stamm, M.; Creton, C. *Macromolecules* **1998**, *31*, 2284–2292.
(2) Schnell, R.; Stamm, M.; Creton, C. *Macromolecules* **1999**, *32*, 3420–3425.
(3) Silvestri, L.; Brown, H. R.; Carrà, S.; Carrà, S. *J. Chem. Phys.* **2003**, *119*, 8140–8149.
(4) Cole, P. J.; Cook, R. F.; Macosko, C. W. *Macromolecules* **2003**, *36*, 2808–2815.
(5) Brown, H. R. *J. Adhes.* **2006**, *82*, 1013–1032.
(6) Zhang, J.; Cole, P. J.; Nagpal, U.; Macosko, C. W. *J. Adhes.* **2006**, *82*, 887–902.
(7) Gutowski, W. S. *J. Adhes.* **2003**, *79*, 445–482.
(8) Wu, S. *Polymer Interface and Adhesion*; Marcel Dekker: New York, 1982; p 111.
(9) Creton, C.; Kramer, E. J.; Hui, C. Y.; Brown, H. R. *Macromolecules* **1992**, *25*, 3075–3088.
(10) Janarthanan, V.; Stein, R. S.; Garret, P. D. *Macromolecules* **1994**, *27*, 4855–4858.
(11) Bucknall, D. G.; Arrighi, V. *Polymer Blends*; Paul, D. R., Bucknal, C. B., Eds.; Wiley-Interscience: New York, 2000; Vol. *1*, p 349.
(12) Brown, H. R.; Char, K.; Deline, V. R.; Green, P. F. *Macromolecules* **1993**, *26*, 4155–4163.
(13) Schaffer, M.; Janarthanan, V.; Deng, Y.; La Scala, J.; Guo, L.; Rafailovich, M.; Sokolov, J.; Stein, R.; Strzhemechny, Y.; Schwarz, S. A. *Macromolecules* **1997**, *30*, 1225–1227.
(14) Hüttenbach, S.; Stamm, M.; Reiter, G.; Foster, M. *Langmuir* **1991**, *7*, 2438–2442.
(15) Lorenz-Haas, C.; Muller-Buschbaum, P.; Ittner, T.; Kraus, J.; Mahltig, B.; Cunis, S.; Krosigk, G. V.; Gehrke, R.; Creton, C.; Stamm, M. *Phys. Chem. Chem. Phys.* **2003**, *5*, 1235–1241.
(16) Xu, Z.; Kramer, E. J.; Edgecombe, B. D.; Fréchet, J. M. *Macromolecules* **1997**, *30*, 7958–7963.
(17) Horiuchi, S.; Yin, D.; Liao, Y.; Ougizawa, T. *Macromol. Rapid Commun.* **2007**, *28*, 915–921.
(18) Reimer, L. *Image Formation in Low-Voltage Scanning Electron Microscopy*; SPIE: Bellingham, WA, 1993.
(19) Jaksch, H.; Steigerwald, M.; Drexel, V. *Microsc. Microanal.* **2005**, *11*, 758–759.
(20) Jaksch, H.; Steigerwald, M.; Drexel, V.; Bihr, H. *Microsc. Microanal.* **2003**, *9*, 106.
(21) Jaksch, H.; Martin, J. P. *Fresenius J. Anal. Chem* **1995**, *353*, 378–382.
(22) Suess, M.; Kressler, J.; Kammer, H. W. *Polymer* **1987**, *28*, 957–960.
(23) Fowler, M. E.; Barlow, J. W.; Paul, D. R. *Polymer* **1987**, *28*, 1177–1184.
(24) Liao, Y.; Nakagawa, A.; Horiuchi, S.; Ougizawa, T. *Macromolecules* **2007**, *40*, 7966–7972.
(25) Higashida, N.; Kressler, J.; Yukioka, S.; Inoue, T. *Macromolecules* **1992**, *25*, 5259.
(26) Fowler, M. E.; Barlow, J. W.; Paul, D. R. *Polymer* **1987**, *28*, 2145–2150.
(27) Li, H.; Yang, Y.; Fujitsuka, R.; Ougizawa, T.; Inoue, T. *Polymer* **1999**, *40*, 927–933.
(28) Hull, D. *Fractography: observing, measuring and interpreting fracture structure topography*; Cambridge University Press: Cambridge, U.K., 1999; pp 139−142.
(29) Man, N.; Okumura, H.; Oizumi, H.; Nagai, N.; Seki, H.; Nishiyama, I. *Appl. Surf. Sci.* **2004**, *231*−*232*, 353–356.
(30) Nagai, N.; Imai, T.; Terada, K.; Seki, H.; Okumura, H.; Fujino, H.; Yamamoto, T.; Nishiyama, I.; Hatta, A. *Surf. Interface Anal.* **2002**, *34*, 545–551.
(31) Sugihara, H.; Oya, K.; Murase, H.; Akabori, K.; Tanaka, K.; Kajiyama, T.; Takahara, A. *Appl. Surf. Sci.* **2008**, *254*, 3180–3183.
(32) Stamm, M.; Hüttenbach, S.; Reiter, G.; Spronger, T. *Europhys. Lett.* **1991**, *14*, 451–456.
(33) Wu, S.; Chuang, H.-K. *J. Polym. Sci., Polym. Phys. Ed.* **1986**, *24*, 143–159.
(34) Xu, Z.; Hadjichristidis, N.; Fetter, L. J.; Mays, J. W. *Adv. Polym. Sci.* **1995**, *120*, 1–50.
(35) Wool, R. P.; Yuan, B. L.; McGarel, O. J. *Polym. Eng. Sci.* **1989**, *29*, 1340–1367.
(36) Onogi, S.; Masuda, T.; Kitagawa, K. *Macromolecules* **1970**, *3*, 109–116.
(37) Horiuchi, S.; Hamanaka, T.; Aoki, T.; Miyakawa, T.; Narita, R.; Wakabayashi, H. *J. Electron Microsc.* **2003**, *52*, 255–266.
(38) Yukioka, S.; Inoue, T. *Polymer* **1992**, *34*, 1256–1259.

MA801607K